Copper Extrusion/Reinjection in Cu-Based Thiospinels by Electrochemical and Chemical Routes

V. Bodenez,[†] L. Dupont,[†] M. Morcrette,[†] C. Surcin,[†] D. W. Murphy,[‡] and J.-M. Tarascon*,[†]

LRCS-UMR 6007, Université de Picardie Jules Verne, 80039 Amiens, France, and University of California, Davis, California 95616

Received February 21, 2006. Revised Manuscript Received June 28, 2006

The electrochemical reactivity of $CuTi_2S_4$ and $CuCr_2S_4$ spinel samples toward Li was studied over a wide range of voltages. Their electrochemical behavior can be decomposed into two steps. For less than two inserted lithium, we emphasized a Li-driven electrochemical displacement reaction that led to the extrusion of copper from lithium, leading to the rocksalt-type structure phases $Li_2Ti_2S_4$ and $Li_{2-x}Cu_{0.3}Cr_2S_4$, whereas conversion reactions were observed beyond $x = 2$. These conversion reactions were shown to have a large rechargeable uptake and release of Li^+ ions (7 per formula unit) that rapidly fade on cycling. Regarding the Cu extrusion, we demonstrated that this process is reversible for the Ti-based spinel upon oxidation through a chemically assisted electrochemical process. For the Cr-based system, a new phase $LiCu_{0.7}Cr_2S_4$ was evidenced to form on oxidation. This difference is explained in terms of band structure considerations and d−sp redox chemistry. Chemical reinjection of Cu into Ti_2S_4 forming the single phase $Cu_xTi_2S_4$ ($0 < x < 1$) from the reaction of Ti_2S_4 powders with an aqueous $CuSO_4 \cdot nH_2O$ solution is also reported. It is shown that traces of H_2S coming from the slight chemical instability of Ti_2S_4 in water are necessary for initiating the chemical reinjection reaction to form $Cu_xTi_2S_4$.

Introduction

Today, rechargeable Li-ion batteries stand as the first power source for portable electronic devices (computer, cell phone). As technological demands increase, so does the search for better electrode/electrolyte materials or new concepts for such batteries. In such a direction, we recently reported a novel, rechargeable positive electrode reaction for $Cu_{2.33}V_4O_{11}$ in Li-ion batteries.[1,2] Both Cu^{n+} and V^{n+} are reduced during the discharge of such cells, Cu being deposited as Cu metal on the surface of the electrode materials and Li^+ intercalated into "V_4O_{11}" to maintain charge neutrality. The reverse process, which has been proven to be very fast, is different. We demonstrate that the mechanism involves first the oxidation of Cu^0 and then an ion-exchange reaction, which have both been proven to be very fast. For $Cu_{2.33}V_4O_{11}$/Li cells, this combination displacement/intercalation (CDI) mechanism gives reversible capacities as high as 270 mA h g^{-1}, more than twice that of electrode materials presently used in commercial Li-ion batteries.

In principle, the CDI reaction offers the possibility of higher energy densities because both the sites occupied by Cu^{n+} ($n = 1$ or 2 for oxides and 1 for sulfides) and any vacant site within the host structure provide potential sites for Li^+, whereas traditional intercalation pathways are able to utilize already vacant sites only. Cu has been previously used as a template to create host structures for subsequent Li intercalation by oxidatively deintercalating Cu.[3] However, such a pathway requires that the defect structure be viable once the Cu is removed. The CDI pathway, which could potentially result in an irreversible structure collapse, offers the possibility of avoiding both a synthesis step and the vacancy of a complete set of cation sites.

As part of an ongoing effort to determine the scope and generality of CDI reactions as the basis for positive electrodes in Li-ion type batteries, we decided to revisit the chemistry of Cu-based thiospinel phases, because previous authors[4−7] have reported some Li-driven copper extrusion without exploring its outcome upon subsequent charges/discharges. In this paper, we report results regarding CuM_2S_4/electrolyte/Li cells (where M = Ti, Cr) with special attention to the interplay between Li^+ and Cu^+ ions during electrochemical redox processes. $CuTi_2S_4$ was chosen for such a study because we know that Cu^+ is mobile and can be removed by oxidation at room temperature to afford a metastable form of c-TiS_2 (or Ti_2S_4) with a defect spinel structure (all tetrahedral A sites vacant and Ti on the octahedral B sites).[8] The resulting Ti_2S_4 reversibly cycles 1 Li/Ti through a single homogeneous phase, $Li_xTi_2S_4$, with Li on the alternate set

* Corresponding author. E-mail: jean-marie.tarascon@sc.u-picardie.fr. Phone: 33 3-2282-7571. Fax: 33 3-2282-7590.

[†] Université de Picardie Jules Verne.

[‡] University of California, Davis.

(1) Morcrette, M.; Rozier, P.; Dupont, L.; Mugnier, E.; Sannier, L.; Galy, J.; Tarascon, J.-M. *Nat. Mater.* **2003**, *2* (11), 755−761.

(2) Poizot, P.; Chevallier, F.; Laffont, L.; Morcrette, M.; Rozier, P.; Tarascon, J.-M. *Electrochem. Solid-State Lett.* **2005**, *8* (4), A184−A187.

(3) Murphy, D. W.; Cros, C.; DiSalvo, F. J.; Waszczak, J. V. *Inorg. Chem.* **1977**, *16*, 3027−3031.

(4) Dedryvere, R.; Olivier-Fourcade, J.; Jumas, J. C.; Denis, S.; Perez Vicente, C. *Chem. Mater.* **2000**, *12*, 1439−1445.

(5) Dedryvere, R.; Olivier-Fourcade, J.; Jumas, J. C.; Denis, S.; Lavela, P.; Tirado, J. L. *Electrochim. Acta* **2000**, *46*, 127−135.

(6) Dedryvere, R.; Denis, S.; Lippens, P.; Olivier-Fourcade, J.; Jumas, J. C. *J. Power Sources* **2001**, *97*−*98*, 204−207.

(7) Imanishi, N.; Inoue, K.; Takeda, Y.; Yamamoto, O. *J. Power Sources* **1993**, *43*−*44*, 619−625.

(8) Schöllhorn, R.; Payer, A. *Angew. Chem., Intl. Ed.* **1985**, *24*, 67.

10.1021/cm060436z CCC: $33.50
Published on Web 08/02/2006

Table 1. All Lattice Parameters Reported as a Function of the Chemical Composition and Various Treatments

formula	cell parameter (Å)	synthesis method
$CuTi_2S_4$	9.978(1)	ceramic method, 700 °C
Ti_2S_4	9.737(1)	chemically made
$Li_2Ti_2S_4$	10.076(1)	electrochemically made
$Cu_{0.45}Ti_2S_4$	9.828(1)	chemically made
$CuCr_2S_4$	9.776(1)	ceramic method, 700 °C
$Li_{1.75}Cu_{0.25}Cr_2S_4$	9.997(1)	electrochemically made
$LiCu_{0.7}Cr_2S_4$	9.94 (1)	electrochemically made

of octahedral sites normally vacant in spinels. Thus, this seemed to provide a straightforward test for the CDI mechanism with the expected reaction

$$2x\mathrm{Li} + \mathrm{CuTi_2S_4} \leftrightarrow x\mathrm{Cu^0} + \mathrm{Cu_{1-x}Li_{2x}Ti_2S_4} \qquad (1)$$

The point of selecting $CuCr_2S_4$ to conduct comparative studies was nested in the fact that it is an anionic mixed-valence system ($Cu^{+}Cr_2^{+++}(S^{--})_3S^{-\bullet}$), whereas $CuTi_2S_4$ is a cation mixed-valence system ($Cu^{+}Ti^{3+}Ti^{4+}S_4^{--}$), therefore providing supplementary information as to the influence of the nature of the host redox centers on the way that CDI type reactions proceed.

For reasons of clarity, the paper will be structured as follows. It will start with an Experimental Section followed by Results comprising two parts related to the studies of $CuTi_2S_4$ and $CuCr_2S_4$. Within each branch, to preserve coherence, we will first address the electrochemical reactivity of the Cu-based thiospinel phases toward Li followed by the chemical simulations of Li/Cu insertion by means of reducing agents. A comparative analysis of the results will then serve as the basis of the Discussion.

Experimental Section

Synthesis. $CuTi_2S_4$ powdered samples were prepared by heating stoichiometric mixtures of Cu, Ti, and S powders at 700 °C (heating rate 0.3°/min) in fused silica ampules for 3 days. Powder purity and crystallinity were monitored by X-ray diffraction (XRD), with a Scintag diffractometer operating in Bragg−Brentano geometry with Cu K_α radiation. X-ray diffraction showed that the resulting black crystalline powder was single-phase $CuTi_2S_4$ with a lattice constant of $a = 9.978(1)$ Å, in agreement with the reported JCPDS file ($a = 9.999$ Å) but different from the recently reported low-temperature rhombohedric form.[9] Single-phase $CuCr_2S_4$ powders were prepared using an experimental protocol similar to that for $CuTi_2S_4$ (but in two steps: 1 day at 400 °C and then 3 days at 700 °C)

For reasons of clarity, the lattice parameters of the phases synthesized through either the ceramic or solution processes are summarized in Table 1.

Chemical Extraction of Cu. The Cu-free spinel Ti_2S_4 phase was obtained, as previously reported,[10] by oxidation of the spinel $CuTi_2S_4$ with Br_2. More specifically, to carry out this reaction, we mixed 300 mg of $CuTi_2S_4$ with 30 mg of Br_2 in 100 mL acetonitrile and stirred the solution at reflux for 2 days. The recovered powders were single-phased with a cubic cell axis nearly similar to that previously reported for Ti_2S_4[9] (9.737(1) instead of 9.739 Å).

Copper Reinjection. A large stoichiometric (25 mL) excess of a $CuSO_4{\cdot}nH_2O$ (1 mol/L) aqueous solution was added to 100 mg of Ti_2S_4 powder phase and stirred for 48 h at room temperature. The lattice parameter from XRD (9.985(1) Å) was similar to that of $CuTi_2S_4$ prepared at 700 °C.

Electrochemistry. The electrochemical cells were made using Swagelok type cells assembled in an argon-filled drybox, using Li metal as the negative electrode, and a Whatman GF/D borosilicate glass fiber sheet, saturated with 1 M $LiPF_6$ in ethylene carbonate (EC) and with dimethyl carbonate (DMC) ((1:1) in weight) as the electrolyte. The positive electrodes contained 10−20 mg of the compound mixed with 15% carbon SP (black carbon from MMM, Belgium).

In situ XRD. An in situ X-ray electrochemical $CuTi_2S_4$/Li cell, similar to the Swagelok cell[11] but with a beryllium window as the current collector on the positive side, was connected to a Mac−Pile system for cycling and placed on the Scintag diffractometer (Cu $K_\alpha = 1.54178$ Å). The cell was cycled at low current density (1 Li in 10 h), and the X-ray powder patterns were collected for every 0.1 reacted Li. Lattice parameter determinations were performed by the full pattern matching method using the Fullprof program.[12]

An in situ X-ray diffraction holder was specifically designed to monitor the chemical reinjection of Cu. The holder consists of a cylindrical Teflon block having at its top a cavity used as a reservoir to contain the $CuSO_4$ solution (1 mol/L) and capped with a Kapton membrane to prevent air contact and solvent evaporation while being transparent to X-rays. The cell was assembled in air by (i) placing a few Whatman GF/D borosilicate glass fiber sheets into the cavity, (ii) soaking them with a 1 M aqueous solution of $CuSO_4$, (iii) adding a few milligrams of Ti_2S_4 on top of the glass fiber sheet, and (iv) tightly sealing it with the Kapton membrane. The cell was mounted on a Bruker D8 diffractometer (Co $K\alpha_{1,2}$ radiation), and XRD patterns were recorded over 48 h, with a 40 min acquisition time for each pattern.

TEM. Transmission electron microscopy (TEM) studies were carried out with an analytical FEG Microscope FEI Tecnai F20 ST operating at 200 kV and equipped with EDAX EDS analysis.

Atomic Absorption Spectrometry. The Li content in lithiated samples recovered from partially discharged/charged $CuCr_2S_4$/Li cells was determined by atomic absorption spectrometry (Analyst 300, Perkin−Elmer). The recovered samples were washed three times in DMC (to ensure the complete wash off of the $LiPF_6$ salt) prior to being removed from the drybox. Afterward, they were dissolved in a nitric acid solution, and water was added to reach solutions of about 3 mg/L of the analyzed element, so as to be in the ideal detection range of the apparatus used.

Results

(1) $CuTi_2S_4$. *Electrochemical Study.* For the anticipated chemistry described in eq 1, we would expect electrochemical cells of the Li/$CuTi_2S_4$ type to show an S-shaped, reversible charge/discharge curve with voltages in the 1.5−3.0 V range. The typical voltage composition trace (Figure 1) for a Li/$CuTi_2S_4$ half-cell discharged at a *C*/10 rate (1 Li in 10 h) shows a staircase variation, with two distinct plateaus located at 0.6 and 0.35 V vs Li that correspond to the uptake of 2 and 6 Li, respectively. To determine the reacting Li-uptake mechanisms associated with these two potential domains and

(9) Soheilnia, N.; Kleinke, K.; Dashjav, E.; Cuthbert, H.; Greedan, J.; Kleinke, H. *Inorg. Chem.* **2004**, *43* (20), 6473−6478.
(10) Sinha, S.; Murphy, D. W. *Solid State Ionics* **1986**, *20*, 81.
(11) Morcrette, M.; Chabre, Y.; Vaughan, G.; Amatucci, S.; J.-B. Leriche; Patoux, S.; Masquelier, C.; Tarascon, J.-M. *Electrochim. Acta* **2002**, *47*, 3137−3149.
(12) Rodriguez-Carvajal, J. *Abstracts of the Satellite Meeting on Powder Diffraction of the XV Congress of the IUCr*, Toulouse, France, 1990; Abstr. 127.

evaluate their reversibility, we conducted cycling experiments by limiting the discharge cutoff voltage to either 0.5 or 0.1 V; this was to separately study the ~0.6 V process and the cumulated ~0.6 and ~0.35 V processes, respectively.

Regarding the first domain, Figure 1a shows that it is reversible. Strikingly, the charge curve completely differs from the discharge one, showing an S shape as opposed to a plateau, with a capacity of about 90% of the discharge. Subsequent discharges show an increase in capacity above 2.0 V, but with the bulk of the capacity remaining below 1 V. Clearly, the chemistry is not as simple as that of eq 1, from which we could have expected an S-shaped first discharge profile. On the contrary, these data are suggestive of the chemistry outlined in eq 2a, which indicates that the end product of discharge is $Li_2Ti_2S_4$ as expected, but with a reaction scheme that does not lead to a mixed Cu/Li phase as witnessed by the presence of a plateau in the $V = f(x)$ curve. Moreover, because of the similarity of the charge curve with respect to the Li/Ti_2S_4 cell data,[11] the large hysteresis observed between charge and discharge, and the presence of the two-phase plateau below 1 V, we suggest that chemical rather than electrochemical reinjection of Cu occurs. Thus, the reaction mechanisms can be described according to eqs 2b and 2c, which occur simultaneously. The increase in capacity above 2.0 V would simply be due to eq 2d or to a slight modification of the Cu amount. On the same plot, we also show that the formation of a single, homogeneous $Li_xTi_2S_4$ phase occurs.

$$x\mathrm{Li}^+ + \mathrm{CuTi_2S_4} + x\mathrm{e}^- \xrightarrow{\text{discharge}} \mathrm{Cu}_{x/2}{}^0 + 0.5\mathrm{Li_2Ti_2S_4} + (1 - 0.5x)\mathrm{CuTi_2S_4} \quad (2a)$$

$$\mathrm{Cu}^0 + \mathrm{Li_2Ti_2S_4} \xrightarrow{\text{charge}} \mathrm{Cu}^0 + \mathrm{Li}_{2-x}\mathrm{Ti_2S_4} + x\mathrm{Li}^+ + x\mathrm{e}^- \quad (2b)$$

$$\mathrm{Cu}^0 + \mathrm{Ti_2Si_4} \xrightarrow{\text{chemical}} \mathrm{CuTi_2S_4} \quad (2c)$$

$$x\mathrm{Li}^+ + \mathrm{Ti_2S_4} + x\mathrm{e}^- \underset{\text{charge}}{\overset{\text{discharge}}{\leftrightarrow}} \mathrm{Li}_x\mathrm{Ti_2S_4} \quad (2d)$$

In situ XRD (Figure 2) was used to verify the validity of the above chemical reactions. On discharge, the important features of those data are (i) the appearance of a copper metal peak (111) at 43.3°, confirming the gradual copper extrusion during the discharge, and (ii) the appearance of a second phase with a slightly larger a axis lattice parameter of 9.985(1) Å as compared to 9.978(1) Å. Although questionable on the extremes, the coexistence of the two phases is unambiguous near $x = 1$. On further discharge, we note a peak-splitting, indicating the evolution of the lattice parameters of the second phase, which becomes unique when $x = 2.1$ Li with an a axis value of $a = 10.076(1)$ Å. This value is close to that reported for $Li_{1.95}Ti_{2.05}S_4$[11] ($a = 10.083$ Å) and is direct proof of the Li electrochemically driven copper extrusion process in accordance with eq 2a. The presence of metallic copper was separately confirmed by a TEM study.

The XRD patterns collected upon recharge for the same in situ cell are displayed in Figure 3. For reasons of clarity, we show only 2θ from 34 to 38° to highlight the variation of the (400) Bragg peak (e.g., the a axis). This peak shifts

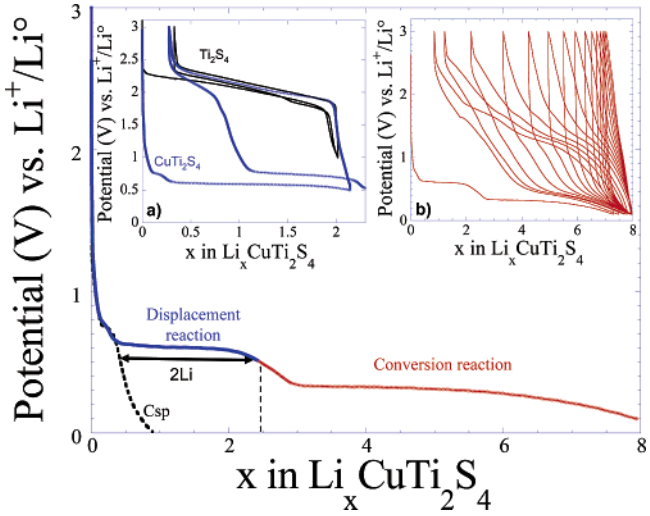

Figure 1. Typical potential−composition trace for a $Li/CuTi_2S_4$ cell (solid line) discharged to 0.1 V at a $C/10$ rate (1 Li in 10 h). Inset: (a) Voltage profile (solid line) for a $Li/CuTi_2S_4$ cell cycled between 0.5 and 3 V rate as compared to the voltage−composition curve for a Li/Ti_2S_4 cell cycled under similar conditions. (b) Potential−composition traces for a $Li/CuTi_2S_4$ cell cycled at a $C/10$ rate between 0.1 and 3 V, shown for the first few cycles.

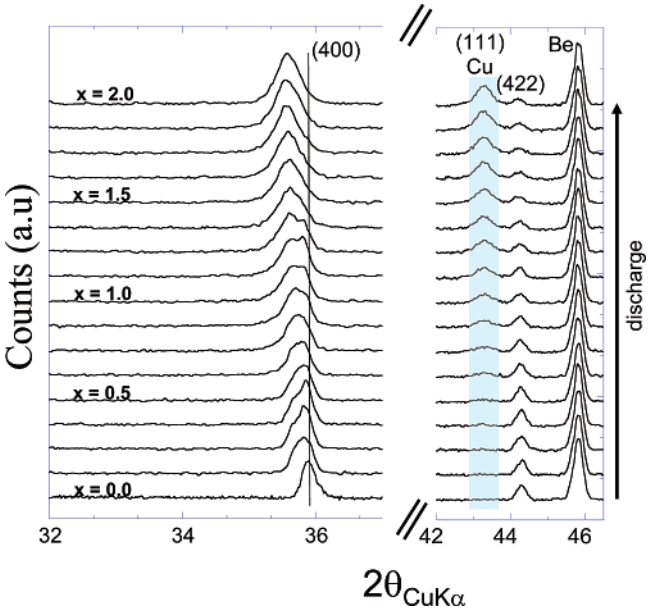

Figure 2. In situ X-ray diffraction patterns collected during the discharge of a $Li/CuTi_2S_4$ electrochemical cell discharge down to 0.5 V at a $C/10$ rate. For reasons of clarity, we present the 2θ ranges only showing the most prominent features, namely the splitting of the (311) and (400) peaks of the mother phase together with the appearance of the Cu (111) peak.

smoothly and continuously to larger 2θ values on charge, indicating a continuous decrease in the a axis value from $a = 10.076(1)$ Å to $a = 10.011(2)$ Å, a value corresponding to the composition $x \approx 0.8$ in the $Li_xTi_2S_4$ solution solid. At that point, another phase appears that has an a axis value of 9.970(2) Å, a value similar to that of $CuTi_2S_4$, indicative of some copper reinsertion into the structure. Although such phase segregation, further confirmed by TEM, is somewhat surprising, it could be nested in some structural considerations and more specifically in a slight competition between Cu^+ and Li^+ ions for the occupancy of the tetrahedral A vs octahedral B spinel sites. However, to check this site competition, we must know the potential at which Cu is reinserted into the structure. This is a difficult task in the

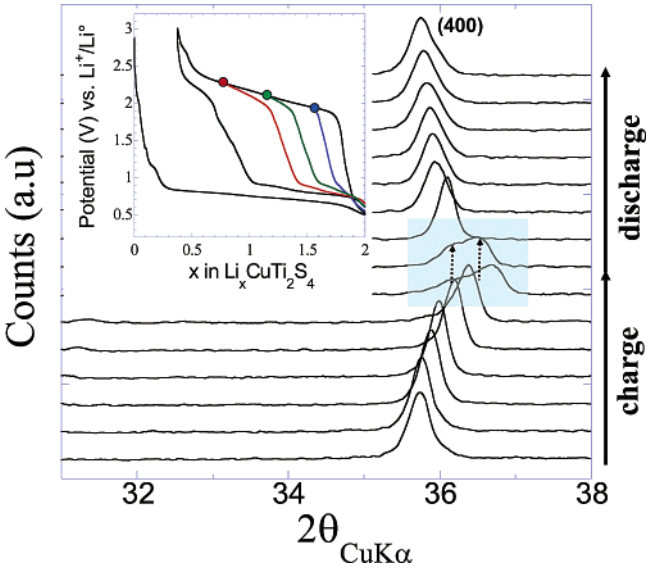

Figure 3. In situ X-ray diffraction patterns collected on the same Li/$CuTi_2S_4$ electrochemical cell as in Figure 2, but on the subsequent charge and discharge cycles. The variation of the (400) Bragg clearly peak showed the coexistence of two phases. The inset shows the second discharge for three samples recharged at various compositions (for 0.4, 0.8, and 1.2 Li amount of Li removed).

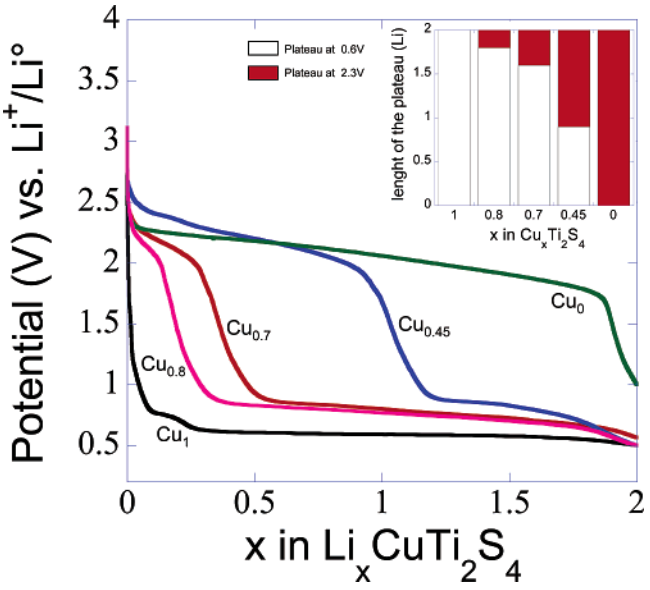

Figure 4. Typical first discharge trace for Li/$Cu_xTi_2S_4$ cells using Cu-leached samples (with $x = 0$, 0.45, 0.7, 0.8, and 1) discharged to 0.5 V. The inset shows the length of the two plateaus (at 2.3 and 0.7 V) for each sample.

absence of a voltage anomaly in the charging curves. We simply note that the more we recharge the cell (Figure 3, inset), the more we can observe the two processes at low (0.9 V) and high (2.3 V) voltages. Therefore, the inability to access the Cu/Li content in our partially recharged samples prevented a detailed explanation of the voltage profile.

To bypass this issue, quantitative chemical extraction of copper was realized by oxidation of the spinel $CuTi_2S_4$ with Br_2. We used EDS analyses to precisely determine the copper content in the materials**.** Figure 4 shows a typical composition trace for a $Cu_xTi_2S_4$/$LiPF_6$/Li cell discharged to 0.5 V. According to Figure 4, for $x = 1$, the plateau is at 2.3 V and for $x = 0$, it is at 0.6 V. In contrast, for intermediary compositions, we observe two plateaus separated by 1.4 V,

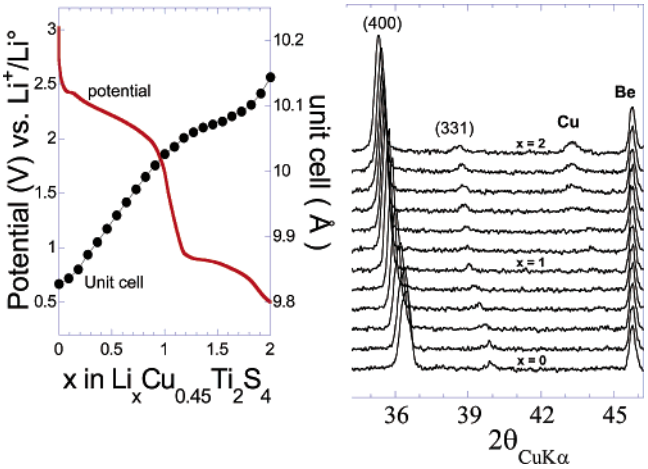

Figure 5. In situ X-ray diffraction patterns collected during the discharge of a Li/$Cu_{0.45}Ti_2S_4$ electrochemical cell to 0.5 V at a *C*/10 rate. For reasons of clarity, we present the 2θ ranges only showing the most prominent features, namely the shift of the (400) peak of the mother phase together with the appearance of the Cu (111) peak.

with capacities dependent on the remaining Cu content, with the largest low-voltage plateau obtained for Cu-rich samples (Figure 4, inset). It is worth noting that we can fill the structure with two times more lithium than vacancies in the copper sites (e.g., 0.4 Li with $Cu_{0.8}Ti_2S_4$, 0.6 with $Cu_{0.7}Ti_2S_4$, and 1.1 with $Cu_{0.45}Ti_2S_4$). The intermediate $Cu_{0.45}Ti_2S_4$ composition, because of its perfectly well-defined plateaus, was selected for in situ XRD studies to monitor structural changes during discharge (Figure 5, right). As before, we present only the 2θ ranges that show the most prominent features, namely a continuous shift of (331) and (400) peaks of the mother phase together with the appearance of the Cu (111) peak. The fully discharged phase has a lattice *a* axis parameter of $a = 10.144(1)$ Å as compared to 9.828(1) Å for the starting phase. Interestingly, the lattice parameter variation is not smooth but presents two sloping *a* axis ranges (Figure 5, left) that cross over at values of *x* corresponding to the 1.4 V voltage drop in the voltage−composition curve, indicative of the existence of two different processes.

We believe the first high-sloping voltage is nested in the insertion of lithium into the free tetrahedral site of the starting $Cu_{0.45}Ti_2S_4$ phase through a solid solution process, whereas the low-voltage phenomena could be indicative of a CDI type reaction, consistent with the appearance of Cu metal. Thus, the overall discharge scheme can be written as follows

$$[Cu_x]_{tet}[Ti^{3+}{}_xTi^{4+}{}_{2-x}]_{oct}S_4 \rightarrow [Li_{2(1-x)}]_{tet}[Cu_x]_{tet}[Ti_{2-x}{}^{3+}Ti_x{}^{4+}]_{oct}S_4 \rightarrow [Li_2]_{oct}[Ti^{3+}{}_2]_{oct}S_4 + xCu^0$$

It is therefore surprising that this change is accompanied by a large voltage drop without drastic structural changes. Interestingly, such a large voltage change was observed upon further lithiation of $LiMn_2O_4$ and was associated with the Mn^{3+} Jahn Teller ions. Thus it could be that Ti^{3+}, also a Jahn−Teller ion, has something to do with the observed voltage drop.

To check whether all the copper could be reinjected on charging, we increased the cell cutoff voltage to 3.7 V (e.g.,

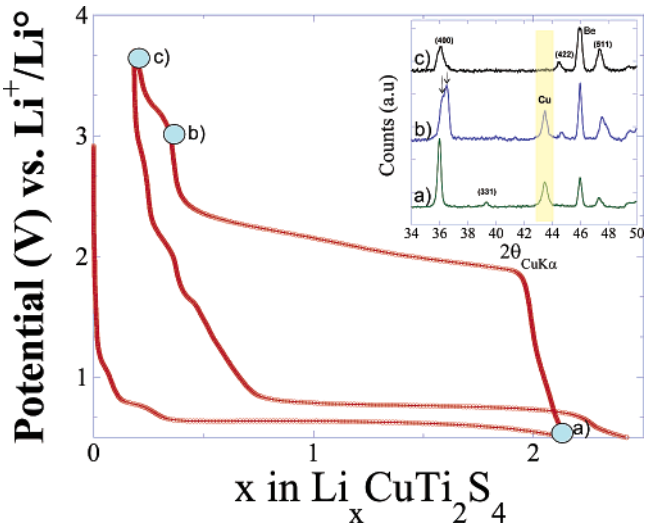

Figure 6. X-ray powder patterns collected for electrodes recovered from $Li/CuTi_2S_4$ cells that were cycled at *C*/10 rates and stopped at potentials denoted by a−c on the voltage−composition curve. Note the disappearance of the Cu Bragg peak for the compound charged up to 3.7 V.

just above the oxidation of copper metal) and observed some extra capacity. This extra capacity could be due to the oxidation of Cu into Cu^+, which can either be ion exchanged with Li into the material or simply migrate in the electrolyte. The former will lead to modifications of the lattice parameters of our compound associated with the increase in its copper content, whereas the latter should not affect the structure, and the overall Cu content within the sample should decrease. To distinguish between the two possibilities, we conducted both TEM (not shown) and XRD measurements for the sample recovered in part c ($V = f(x)$ curve, Figure 6). The XRD powder pattern (Figure 6, inset) not only reveals the absence of the (111) Cu Bragg peak but also indicates a single-phase product with an *a* axis of 9.977 Å like $CuTi_2S_4$, unambiguously confirming the possibility of fully reinjecting copper into the material. Thus, as expected, the following discharge bears some similarity to the first discharge with only one plateau located near 0.7 V vs Li^+/Li^0 (200 mV above the plateau of the first discharge). In light of such results, it seems likely that the two phases observed near 3 V on charge (Figure 6, inset b) are rooted in the inability, at a specific Cu/Li ratio, to occupy the same adjacent octahedral sites as Li alone does.

Finally, we explored the reversibility of $Li/CuTi_2S_4$ cells down to 0.2 V. Note (Figure 1, inset b) that there is a Li uptake of 8 Li^+, out of which 7 can be removed on the following charge, leading to a 7 Li rechargeable process, but the capacity decays rapidly on cycling. Such a large capacity implies that the displacement reaction occurring down to 0.5 V is followed by a conversion type reaction that enlists the full reduction of Ti^{3+} in Ti metal according to the following reaction

$$Li_2Ti_2S_4 + 6Li^+ + 6e^- \rightarrow 2Ti^0 + 4Li_2S$$

The presence of Li_2S and its disappearance upon the following charge were confirmed by both X-ray diffraction and HRTEM studies, but we were unable to confirm the presence of crystalline Ti particles by these same methods. The partial solubility of Li_2S into the 1 M $LiPF_6$ EC-DMC electrolyte previously mentioned in the literature[13] is most likely responsible for the rapid cell-capacity decay.

Chemical Insertion of Cu. In contrast to Li insertion, the insertion of Cu into cubic Ti_2S_4 has not been reported. Nevertheless, there are some literature reports dealing with the intercalation of copper between the layers of the hexagonal TiS_2 phase using either mechanical alloying[14] or low-temperature (50 °C) electrochemical methods.[15] Here, we report a chemical method enabling the preparation of a $Cu_xTi_2S_4$ spinel type structure by immersion of Ti_2S_4 in a two-fold excess of aqueous $CuSO_4 \cdot nH_2O$ (1 mol/L) for 48 h under constant stirring at room temperature. This reaction time is usually sufficient to produce $CuTi_2S_4$ powders having, as deduced by XRD, lattice parameters similar to those of $CuTi_2S_4$ made at 700 °C. It is worth noting that attempts at intercalating copper into the hexagonal TiS_2 phase using a similar experimental protocol (2 days, 1 M $CuSO_4$ solution) were unsuccessful, even when increasing the reaction temperature to 50 °C. This is indicative of a much faster Cu insertion process into 3D Ti_2S_4 than in 2D TiS_2.

To grasp some insight in the copper reinjection mechanism into Ti_2S_4, we designed experiments so as to continuously monitor in both semi in situ and in situ manners the degree of advancement of the Cu insertion reaction. Every 12 h, 2.5 mL of $CuSO_4$ solution was added and the pH was measured, followed by withdrawals operated in order to recover, after filtration, powders for XRD. The *a* lattice parameter gradually increases (Figure 7, inset a) when the added amount of $CuSO_4$ is increased to reach a final value of 9.97(1) Å, indicative of the formation of $CuTi_2S_4$. The pH of the solution abruptly decreases during the reaction to reach a stable value of 3.5 that is sustained throughout the reaction. An H_2S-like smell was noted in the early stage of the reaction, but disappeared with increasing reaction time. For reasons of toxicity, we completed all experiments under an extractor hood. We also monitored the reaction using an in situ X-ray diffraction cell (Figure 7). For reasons of clarity and conciseness, we show the 2θ (50−54°) region only, highlighting the time evolution of the (440) Bragg peak. This peak continuously shifts toward lower 2θ angles, confirming, as for the semi in situ experiment, a continuous increase in the *a* cubic axis parameter and indicative of the presence of a $Cu_xTi_2S_4$ complete solid solution for $0 \leq x \leq 1.0$.

It is interesting to consider how the chemical insertion of Cu by $CuSO_4$ solution might occur. Both Ti ($Ti^{4+} \rightarrow Ti^{3+}$) and Cu ($Cu^{2+} \rightarrow Cu^+$) are being formally reduced in the reaction. Thus, whatever the detailed mechanism, something must be oxidized. Among the possible candidates are H_2O or SO_4^{2-}. The possible reactions (all written as reductions below with standard potentials) are as follows

$$S_2O_8^{2-} + 2e^- = 2SO_4^{2-} \quad E = 2.0 \text{ V}$$

$$H_2O_2 + 2H^+ + 2e^- = 2H_2O \quad E = 1.776 \text{ V}$$

$$O_2 + 4H^+ + 4e^- = 2H_2O \quad E = 1.23 \text{ V}$$

All show *E* values higher than the $E = 1.06$ V of the $Br_2 + 2e^- = 2Br^-$ that was used to remove Cu through oxidation

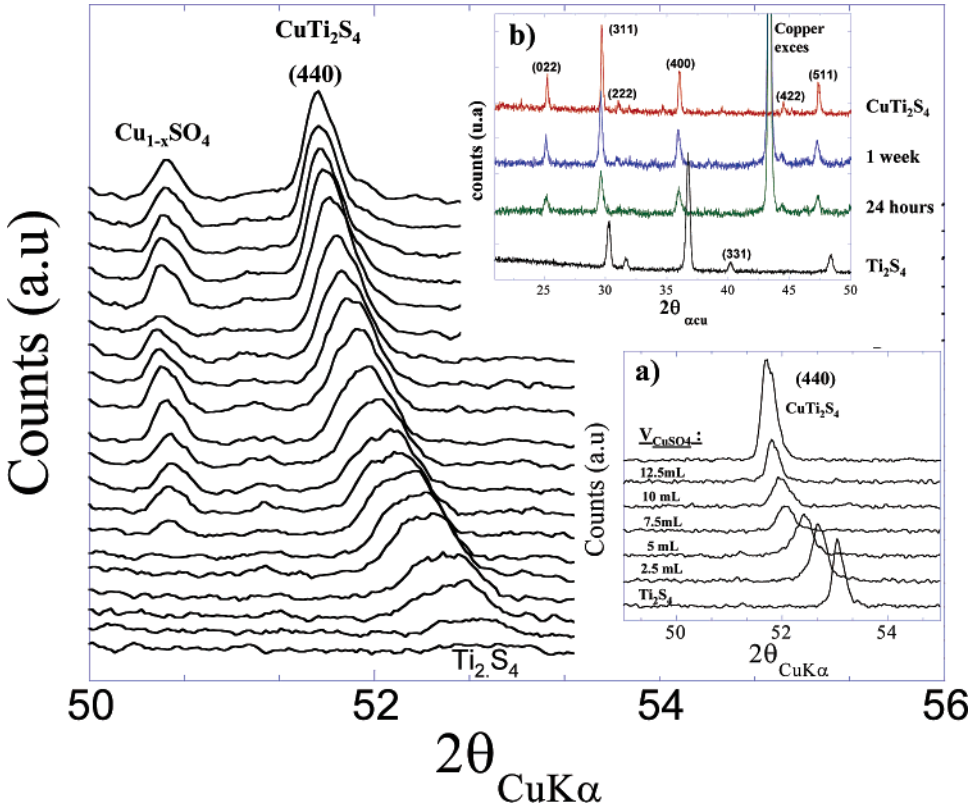

Figure 7. (Left) Zoom of the (440) peak evolution during the X-ray in situ monitoring of the reinjection of copper into Ti_2S_4 in aqueous media using a specially designed sample holder. Inset: (a) Semi in situ X-ray monitoring of the Ti_2S_4 (440) peak as a function of increasing amounts of $CuSO_4$ solution (1 mol/L). (b) X-ray powder pattern evolution of a pelletized Cu + Ti_2S_4 powder mixture as a function of time at 55 °C.

of $CuTi_2S_4$ and are therefore unlikely. Another scenario has to be proposed. In light of the H_2S smell previously mentioned, we decided to investigate the chemical stability of Ti_2S_4 in H_2O. Ti_2S_4 (500 mg) was dropped into neutral water, and the pH was monitored. An instantaneous decrease in pH was noted upon addition of the powders. After 12 h of soaking time in the solution at a pH of 3.5, the mixture was centrifuged; both the powders and the supernatant were recovered for XRD analysis and H_2S detection, respectively. The XRD pattern of the recovered powder still reveals the presence of Ti_2S_4. Qualitative analysis for H_2S traces was done by adding a few milligrams of lead acetate, cadmium nitrate, or manganese sulfate to the milky supernatant. The instantaneous formation of black, yellow, and orange precipitates was indicative of the formation of H_2S, HS^-, or S^{2-}, respectively. Part of the recovered powder was placed into freshwater, and the above analysis was conducted again after 12 h of soaking. The presence of H_2S was observed again, clearly indicating a continuous and slight decomposition of the material in water. That is not surprising, according to the equation $S + 2H^+ + 2e^- = H_2S(aq)$ $E = 0.142$ V. In contrast, we found that $CuTi_2S_4$ was very stable under the same conditions. Thus, in light of these observations, we suggest that the H_2S generated from the reaction of H_2O and Ti_2S_4 acts as the reducing agent facilitating the formation of $CuTi_2S_4$. The same decomposition explains the rapid decrease in pH (according to the reactions below) observed at the early stage of copper reinjection

$$\text{decomposition} \qquad Ti\,S_2 \rightarrow Ti^{4+} + 2S^{--}$$

$$H_2S \text{ formation} \qquad 2H_2O + S^{--} \rightarrow H_2S + 2OH^-$$

$$\text{pH} \qquad H_2S \rightarrow [HS^-, H^+];\ Ti^{4+} + nOH^- \rightarrow Ti(OH)_n$$

Finally, in light of the above findings, we attempted to and succeeded (Figure 7, inset b) in reinserting Cu into Ti_2S_4 to prepare $CuTi_2S_4$ by using a solid-state route and reacting a pellet made from stoichiometric amounts of Ti_2S_4 and metallic Cu powders for 24 h at 55 °C. This not only further confirms the high Cu mobility into the spinel Ti_2S_4 but also supports the feasibility of eq 2c.

(2) $CuCr_2S_4$. *Electrochemical Study.* The voltage−composition curve for a Li/$CuCr_2S_4$ cell discharged down to 0.5 V (Figure 8) shows, as for the Li/$CuTi_2S_4$, a highly rechargeable process involving the uptake of 8 Li per formula unit on the first discharge followed by the removal of 7 Li on the subsequent charge. As for $CuTi_2S_4$, this large capacity is indicative of a full reduction of Cu^{1+} and Cr^{3+} ions to metallic Cu^0 and Cr^0, and of the $S^{-\bullet}$ anion into S^{--} respectively. The reduction of both cations and anions accounts for the uptake of 7 and 1 e^- that are 8 Li^+ ions altogether, respectively. Thus a conversion reaction process, as encountered for other binary/ternary oxides structures and free of structural sites/vacancies, appears at first to govern the reactivity of $CuCr_2S_4$ toward Li. This was directly

(13) Han, S.-C.; Kim, K.-W.; Ahn, H.-J.; Ahn, J.-H.; Lee, J.-Y. *J. Alloys Compd.* **2003**, *361*, 247−251.
(14) Kusawake, T.; Takahashi, Y.; Ohshima, K. *Mater. Res. Bull.* **1998**, *33* (7), 1009−1014.
(15) Ohtani, T.; Tsubota, A.; Ohshima, K. *Mater. Res. Bull.* **1999**, *34*(7), 1143−1152.

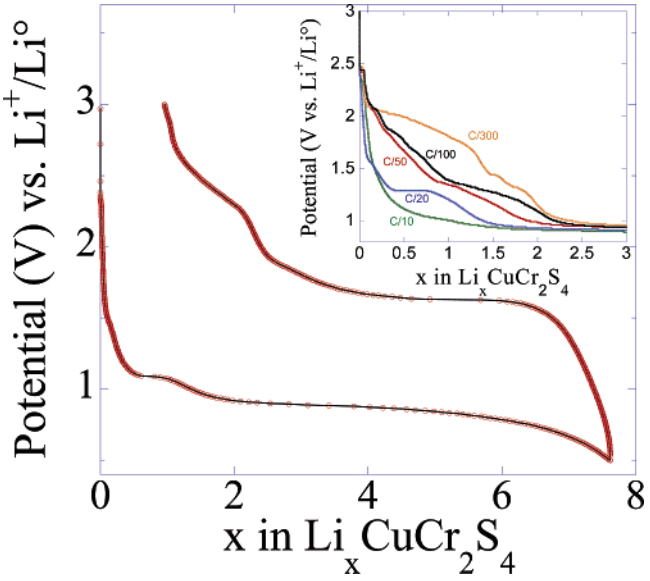

Figure 8. Typical potential−composition trace for a Li/$CuCr_2S_4$ cell cycled between 0.5 and 3 V at a *C*/20 rate. The inset shows the cycling data for the same cell discharged down to 0.9 V at various discharge rates.

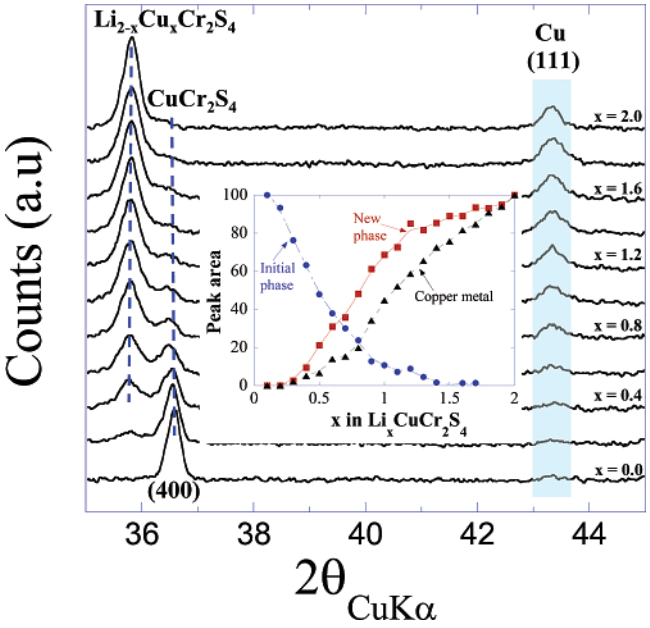

Figure 9. In situ X-ray diffraction patterns collected at various stages of discharge of a Li/$CuCr_2S_4$ electrochemical cell cycled at a *C*/10 rate. Only the ranges of 2θ corresponding to the evolution of the $CuCr_2S_4$ (400) Bragg peak and to the appearance of metallic Cu have been reported. Inset: area evolution of the (400) Bragg peak for the mother phase ($CuCr_2S_4$), the new phase $Li_{2-x}Cu_{0.3}Cr_2S_4$, and the metallic copper (111) peak.

confirmed by in situ X-ray studies (not shown here for reasons of length), which have indicated for the fully discharged sample (e.g., 0.02 V) a somewhat featureless XRD with the exception of two Bragg peaks located near $2\theta = 27$ and 43.3° and corresponding to the presence of Li_2S and metallic Cu. As expected for conversion reactions, we noted the repeated appearance and disappearance of both Li_2S and Cu upon subsequent discharge/charge cycles between 0.02 and 3.0 V.

Nevertheless, as for $CuTi_2S_4$, the first discharge trace occurs stepwise, with an initial rapid decay of the voltage that reaches a first plateau at about 1.25 V, followed by a second voltage decay that reaches, near $x = 2$, a long second "pseudoplateau" located around 0.8 V that extends to $x = 8$. The first plateau, in contrast to the second, was shown to be very sensitive to the cell discharge current rate (Figure 8, inset), with a shift to higher potentials at lower rates, indicative of the presence of two or more competing reduction reactions with different kinetics, as will be discussed in a forthcoming paper.

To precisely identify the origin of these plateaus, we have performed in situ X-ray electrochemical measurements, first focusing on the first plateau. A Li/$CuCr_2S_4$ was assembled, placed on the Scintag diffractometer, discharged to $x = 2$ at low current density (1 Li in 20 h), and then recharged. Figure 9 shows the XRD diagrams recorded during the discharge between $x = 0$ and $x = 2$. Once Li ions begin to be electrochemically injected, a new set of Bragg peaks appear and grow on the left of those corresponding to $CuCr_2S_4$. This new set, which becomes unique as x approaches 2, was indexed similarly to $CuCr_2S_4$, as a cubic unit cell with an a axis of 9.997(1) Å instead of 9.776(1) Å. Concomitant with the growth of this new phase was the onset of another extra peak located at $2\theta = 43.3°$ that corresponds to the (111) Bragg peak of metallic copper. Thus, as for $CuTi_2S_4$, Li initially reacts with $CuCr_2S_4$ through a CDI reaction process concomitantly leading to the extrusion of copper and the growth of a new $Li_{2-x}Cu_xCr_2S_4$ phase. To more precisely understand the mechanism of extrusion of copper, we discharged a Li/$CuCr_2S_4$ cell down to 0.9 V; we monitored the evolution of the integrated area of the (111) peak of elemental copper and plotted it as a function of the Li uptake number (Figure 9, inset). We observed a continuous increase in the peak area and concluded that there is a gradual copper extrusion. Although the above formula leads to complete copper removal by $x = 2$, EDS analysis indicates an atomic copper content of 0.3 ± 0.1. This, combined with a Li content of 1.8 ± 0.1 (as deduced by atomic absorption analysis), implies that the single-phase material, within the accuracy of the measurement (±0.1), will lead to the composition $Li_{1.75}Cu_{0.25}Cr_2S_4$. The same amount of Cu was found for a sample discharged to $x = 2.5$ (e.g., pertaining to the two-phase domains), consistent with the beginning of the conversion reaction associated with the formation of Li_2S.

In parallel, a chemical simulation of the electrochemical discharge was attempted using *n*-butyllithium 1.6 M in hexane as the reducing agent (potential of +1 V vs Li^+/Li). More specifically, 100 mg of $CuCr_2S_4$ was mixed with a large excess (1.5 times assuming the reactivity of two Li) of *n*-butyllithium in hexane. This mixture was stirred for 72 h at 50 °C. Once washed three times in a hexane solution, the recovered powders were examined by XRD, which revealed the coexistence of a rocksalt-type phase with a cell parameter of 10.01(1) Å (similar to the compound obtained by electrochemical discharge) with a copper phase, as deduced from the appearance of the Cu(111) Bragg peak near $2\theta = 42.5°$ and implying that the chemical reduction proceeds according to the reaction below

$$CuCr_2S_4 + C_4H_9{-}Li \rightarrow Li_yCu_{1-x}Cr_2S_4 + xCu^0 + (y/2)\text{octane}$$

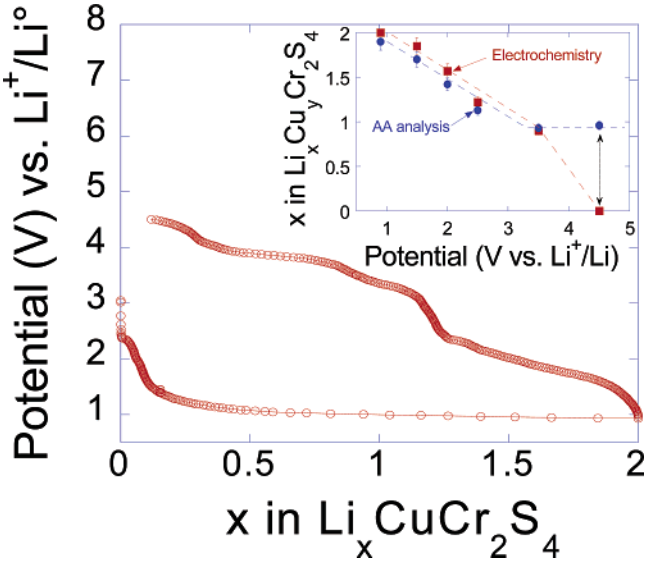

Figure 10. Potential−composition trace is shown for a Li/$CuCr_2S_4$ cell that was charged and discharged at a *C*/10 rate between 0.9 and 4.5 V. The Cu, Cr, and Li contents were monitored during the cell recharge by conducting atomic absorption analyses on samples recovered from cells that were discharged to 0.9 V and recharged at various voltages. The inset shows the Li content values as deduced by both the potential−composition curve and atomic absorption spectroscopy.

with $x = 0.75$ and $y = 0.1.75$, as determined by AA and EDS measurements, respectively.

Surprisingly, regardless of the way we made the discharged material (chemically or electrochemically), we could not remove more than 1 Li per formula unit even when increasing the voltage to 3.5 V (Figure 10), as compared to about 2 for $CuTi_2S_4$ (Figure 1, inset a). Through the semi in situ XRD patterns recorded on charge (Figure 11), we observed no change in the peak position up to 2 V; as the potential increased from 2 to 4.5 V, we then noted a splitting of the Bragg peaks, likely induced by a decrease in symmetry of the spinel cell (F-type cell), into a tetragonal I lattice. Because of the weak and broad peaks recorded on the XRD pattern, only a rough fitting could be calculated. The accuracy of the values needs to be confirmed by an electron diffraction study (under progress). The *c* cell parameter is unchanged ($c = 9.99$ Å compared to 10.00 Å for the spinel), whereas the cell parameter is $a_{\text{tetragonal}} \approx a_{\text{cubic}}\sqrt{2}/2 = 6.95$ Å. Only a cell distortion could be explained by a competition between the copper cations reentering the host structure and the lithium still present, and it implies that the extra cations are located in the octahedral sites. This type of distortion was already reported[15] during the lithiation of $LiMn_2O_4$ leading to $Li_2Mn_2O_4$, where lithium predominantly occupies the octaedral sites.

When the potential reaches 4.5 V, the distortion is lower and it is difficult to observe the splitting of the Bragg peaks. For this reason, the final phase was indexed on the basis of a cubic unit cell with $a = 9.94(1)$ Å. The (111) Bragg peak corresponding to copper metal remains constant at the early stage of the process, then progressively decreases as the cell voltage rises to 3.5 V. Parallel HRTEM experiments performed on the discharged (V = 0.9 V) and partially recharged (3.5 and 4.5 V) sample confirm the single-phase character of the 3.5 V sample.

To be as precise as possible on the chemical composition at various states of charge, we combined EDS and atomic absorption studies. First, EDS analyses were made in several stages during the reoxidation process (discharge at 0.9 V, recharged at 3.5 and 4.5 V) to determine the copper,

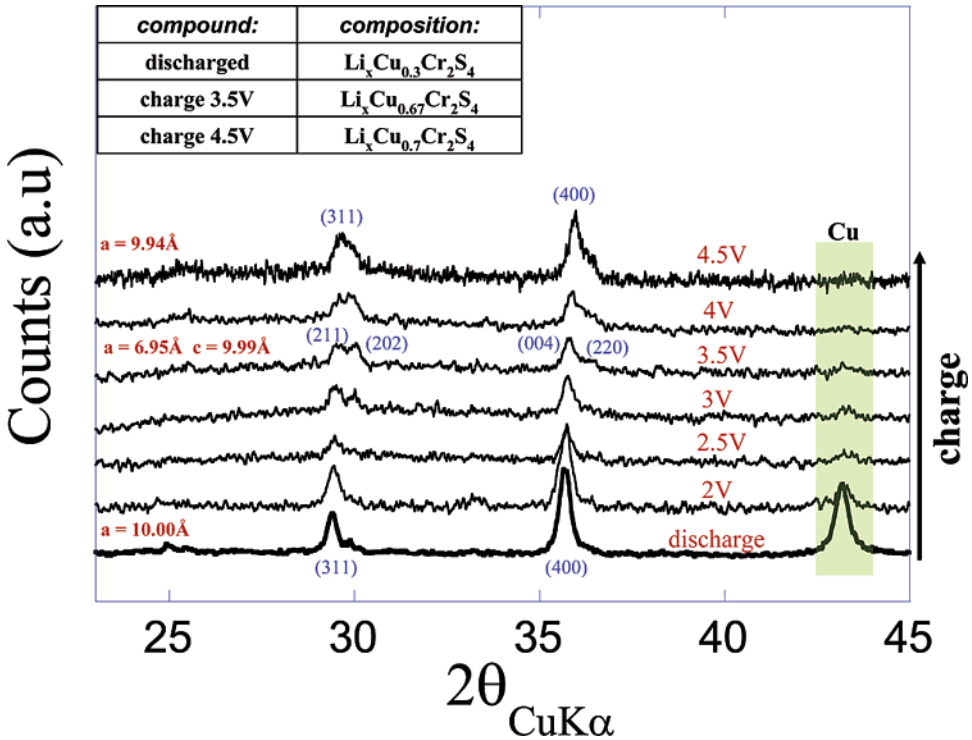

Figure 11. Semi in situ X-ray diffraction patterns collected at various stages of recharge of a Li/$CuCr_2S_4$ electrochemical cell first discharged at a *C*/10 rate until 0.9Li. Only the ranges of 2θ corresponding to the evolution of the $CuCr_2S_4$ (400) and the (111) Bragg peak of metallic Cu are shown. The inset shows EDS analyses for the initial discharged compound and the recharged 3.5 and 4.5 V.

chromium, and sulfur composition (Figure 11, inset). This experiment confirms the reintroduction of copper during the charge and that the ratio S/Cr remains the same. Moreover, there are no drastic differences between the composition at 3.5 and 4.5 V. They both show a ratio of 10/30/60 in Cu/Cr/S. Because the sulfur/chromium ratio is constant (S/Cr = 2) during the entire cycle, we can determine the concentration of lithium in the compound by measuring the proportion of Li/Cr by atomic absorption spectrophotometry. The Figure 10 inset shows the Li/Cr ratio determined by atomic absorption spectrophotometry and the electrochemical method for various potentials during the reoxidation of the compound. For $x \geq 1$, we observe a good agreement between the two methods. In contrast, for voltages greater than 3.5 V, the lithium proportion in the spinel does not change, indicating that we cannot remove more than 1 Li per formula unit. The Cu content evolution upon recharge, as deduced by EDS measurements, increases from 0.3 to about 0.7 ($Li_{1.0}Cu_{0.7}Cr_2S_4$) as the cell voltage changes from 1 to 3.5 V, in agreement with the decrease in the Cu peak intensity as deduced from XRD (Figure 11). Moving from $Li_{1.75}Cu_{0.25}Cr_2S_4$ to $Li_{1.0}Cu_{0.7}Cr_2S_4$, with the removal of only one electron as indicated by the voltage composition curve, is indicative of a complex oxidation path, possibly involving the oxidation of 1 S^{2-} into 1 $S^{-\bullet}$ and an internal redox process leading to the oxidation of Cu into Cu^{1+} by the pyrite-type bonds (S^{0-}) according to the reactions below.

$$Li^{+}_{1.75}Cu^{+}_{0.25}Cr_2^{3+}S^{2-}_{4} \rightarrow Li^{+}_{1.0}Cu^{+}_{0.25}Cr_2^{3+}S^{2-}_{3.25}S^{-}_{0.75} \rightarrow Li^{+}_{1.0}Cu^{+}_{0.7}Cr_2^{3+}S^{2-}_{3.7}S^{-}_{0.3}$$

Increasing the charging voltage to 4.5 V did not change either the Cu or the Li content, implying that within this potential range, there is most likely an oxidation of the remaining nonreacted extruded copper into electrolyte-soluble Cu^{+} species, in agreement with the total disappearance of the Cu peak on the XRD of the material oxidized to 4.5V. Nevertheless, to verify the validity of this assumption, we used a four-electrode homemade cell with two electrodes for galvanostatic cycling of the cell and the other two for cyclovoltamperometry on the electrolyte to detect the presence of dissolved Cu^{+} species. Evidence of dissolved Cu was detected until the cell charge cutoff voltage exceeded 3.8 V.

Discussion

We have reported on the reactivity of two thiospinel phases ($CuCr_2S_4$ and $CuTi_2S_4$) toward Li down to low voltages. We found that both phases behave in a somewhat similar manner, because the first discharge initially enlists a displacement reaction leading to copper extrusion and the formation of $Li_2Ti_2S_4$ or $Li_{1.75}Cu_{0.25}Cr_2S_4$ phases, reversible for the former and partially reversible for the latter, as long as we do not extend the cycling beyond $x = 2$. We have shown that pursuing discharge further is associated with the onset, near 0.3 and 0.9 V for the Ti- and Cr-based spinel phases, of a conversion-type reaction leading to large Li uptakes resulting in the formation of a composite electrode containing metallic elements embedded in a Li_2S matrix electrode that can be cycled. No extended cycling was pursued with these materials because of the well-known fact that Li_2S is slightly soluble in the electrolyte.

The difference between the voltages of the conversion reactions for the Ti- and Cr-based thiospinel can be accounted from thermodynamic calculations. Indeed, from the Gibbs free enthalpy of reactions, $M_xS_y + 2ye^{-} + 2yLi^{+} \leftrightarrow xM^0 + yLi_2S$, one can predict the equilibrium potentials by using the well-known Hess and Nernst laws. By using thermodynamic data[17] for the calculations, we found $E_{eq}(Ti_xS_y/Ti^0) = 0.867$ V vs Li/Li^{+} compared to 1.447 V for $E_{eq}(Cr_xS_y/Cr^0)$ (at 298 K and under ambient pressure). The 0.6 V difference between the observed and calculated plateau voltage values is simply rooted in kinetic limitations. Such a voltage difference can be viewed as the energetic barrier to initiating the first electrochemical reduction step. We have shown that it is a function of the ionocovalency of the M−X bonding and is higher for oxides (1 V for CoO)[17] than chalcogenides (0.6 V for CoS). Thus, the observed 0.6 V falls nicely into the line of our previous work on conversion reactions.

Regarding the partial reversibility of the charging process according to eqs 2b and 2c for the Cr-based thiospinel as compared to the Ti-based one, it can be explained in terms of d−sp redox chemistry. Briefly, a d−sp redox process occurs when the respective positions of the anionic antibonding sp levels and cationic d levels lie at similar energies. Such a situation, well-documented by Rouxel et al.,[18,19] is favored with lowering the anionic electronegativity (e.g., going from O to S, Se, and Te) and thereby frequently encountered with heavier chalcogenides rather than with oxides. Furthermore, lowering the electronic d levels (e.g., in going from Ti, V to Cr for instance) can lead to overlap and provoke instantaneous d−sp redox chemistry. For such reasons, $CuCr_2S_4$ appears as an anionic mixed-valence system ($Cu^{+}Cr_2^{+++}(S^{--})_3S^{-\bullet}$), whereas $CuTi_2S_4$ is a cation mixed valence system ($Cu^{+}Ti^{3+}Ti^{4+}S_4^{--}$). In the case of $CuTi_2S_4$, the d titanium levels are high enough to stabilize the 4^{+} oxidation state, whereas in moving to chromium, the d levels are lower in energy so that they fall into the sp band. In short, there is hybridization of the metal−sulfur orbitals that simply results in a redistribution of the molecular orbital between the Cr 3d and sulfur sp atomic orbital, as visualized in the proposed band structure schematic (Figure 12) drawn in the spirit of Rouxel's work. The insertion of Li into this compound will result in the reduction of Cu^{+} to Cu^0 together with the reduction of ($S^{-\bullet} + e^{-} \rightarrow S^{--}$), leading to the $Li_{1.75}Cu_{0.25}Cr_2S_4$ phase. Basically, on charge, as Li is removed from the $Li_{1.75}Cu_{0.25}Cr_2S_4$ phase, we have a merging of the metal d band into the sulfur sp band so that we have a partial filling of the d cationic levels and simultaneous depopulation

(16) Thackenay, M.; David, W. I.; Goodenough, J. B. *Mater. Res. Bull.* **1983**, *18*, 461−472.
(17) Poizot, P.; Laruelle, S.; Grugeon, S.; Dupont, L.; Beaudoin, B.; Tarascon, J.-M. *C. R. Acad. Sci., Ser. IIc: Chim.* **2000**, *3* (8), *681−691*.
(18) Rouxel, J.; Tournoux, M. *Solid State Ionics* **1996**, *84* (3−4), 141−149.
(19) Rouxel, J. *Curr. Sci.* **1997**, *73* (1), 10.

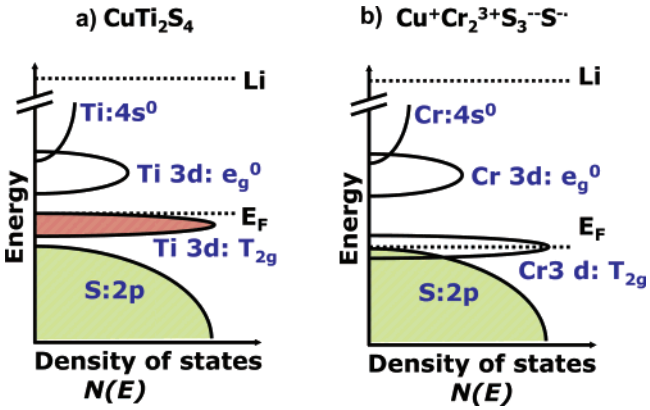

Figure 12. Schematic of the band structure of (a) $CuTi_2S_4$ and (b) $CuCr_2S_4$ as deduced by analogies to those drawn for layered TiS_2 by Rouxel et al.[18,19]

of the top of an sp anionic band, explaining the presence of holes in the sulfur band.

An unanswered question deals with the phase composition of the fully discharged $Li/CuCr_2S_4$ or $Li/CuTi_2S_4$ cells (e.g., at $x = 8$). XRD and TEM data indicate (i) that the fully discharged composite electrode was made of Cu nanoparticles embedded in a Li_2S matrix with no evidence of either Ti or Cr metal nanoparticles, and (ii) that some Cu nanoparticles are still present in the charged (3 V) electrode composite. The persistence of Cu nanoparticles in the fully charged state seems at least consistent with our electrochemical data that do not show any electrochemical signature suggesting the presence of a Cu_xS_y. Lacking information about the state of Cr and Ti in both fully discharged and charged electrodes as well as the outcome of Cu in the fully charged composites, it is too early to further speculate on the presence of a conversion reaction mechanism. Techniques including XANES, EELS, and EXAFS are presently being used to identify the environment as well as the valence state of the Cu, Ti, and Cr ions as a function of the state of charge/discharge of the composite electrodes and sort out the conflicting various models.[20−23]

Overall, the electrochemical reactivity of the Cu-based thiospinel phase toward Li, besides confirming the possibility of rechargeable displacement reactions associated with Cu extrusion/reinjection, has enabled the synthesis of new phases. Furthermore, Cu-based sulfide/selenide phases having either layered or 3D structures are presently being studied to further determine how the effect of Cu^+ mobility and/or electronic structure governs the feasibility of displacement reactions so as to create the necessary basis for developing a strategic synthesis approach for new electrode materials.

Acknowledgment. The authors thank C. Masquelier, D. Larcher, F. Sauvage, P. Poizot, and B. Dunn for helpful discussions. Vincent Bodenez is indebted to the Conseil Régional de Picardie for financial support.

CM060436Z

(20) Sukhetsky, Yu. V.; Soldatov, A. V.; Gusatinskii, A. N. *Physica B* **1992**, *176*, 219−221.
(21) Siberchicot, B. *IEEE Trans. Magn.* **1993**, *29* (6), 3249−3251.
(22) Kimura, A.; Matsuno, J.; Okabayashi, J.; Fujimori, A.; Shishidou, T.; Kulatov, E.; Kanomata, T. *J. Electron Spectrosc. Relat. Phenom.* **2001**, *114−116*, 789−793.
(23) Benco, L.; Barras, J. L.; Atanasov, M.; Daul, C.; Deiss, E. *J. Solid State Chem*. **1999**, *145* (2), 503−510.